Chemical Science

ROYAL SOCIETY OF CHEMISTRY

EDGE ARTICLE

View Article Online
View Journal

Cite this: DOI: 10.1039/d5sc03946k

All publication charges for this article have been paid for by the Royal Society of Chemistry

Scalable synthesis of a low-cost Zn–MOF with a nonpolar pore surface for efficient separation of methanol-to-olefin products

Yingying Zhang,[a] Suyun Deng,[a] Xingye Cui,[a] Jixiang Yue,[a] Hongliang Huang,[c] Chaozhuang Xue,*[b] Huajun Yang*[a] and Lei Gan*[a]

Received 30th May 2025
Accepted 15th September 2025

DOI: 10.1039/d5sc03946k

rsc.li/chemical-science

The pursuit of scalable metal–organic framework (MOF) adsorbents for efficient one-step purification of C_2H_4 and recovery of C_3H_6 holds significant importance for practical applications. It is desirable to incorporate high separation efficiency along with other key norms such as easy scalability, economic feasibility, and eco-friendliness into a single MOF structure. However, this presents a formidable challenge due to the high cost of specially designed ligands, rigorous synthetic conditions, and typically lengthy reaction times. Herein, we present a scalable MOF adsorbent denoted as Zn-hba decorated with a nonpolar pore surface, which successfully integrates all the aforementioned norms. Zn-hba exhibits selective uptake for C_2H_6 and C_3H_6 over C_2H_4 with exceptional selectivity and record-high C_3H_6 and exceptional C_2H_6 uptake at low pressure, allowing for one-step purification of C_2H_4 and recovery of C_3H_6 from a ternary mixture of $C_2H_6/C_2H_4/C_3H_6$. Importantly, Zn-hba is synthesized with a high yield of 42% using commercially available cheap reagents such as zinc acetate, 4-hydroxybenzoic acid, methanol and *n*-amyl alcohol in only 12 hours. The total cost for producing each gram of this adsorbent is as low as $0.14, comparable to that of commercial zeolites and nearly one-tenth the cost of the benchmark MOF MAC-4.

Introduction

Ethylene (C_2H_4) and propylene (C_3H_6), primarily produced from hydrocarbon cracking and the methanol-to-olefin (MTO) reaction, are essential feedstocks for the production of downstream chemicals.[1,2] A crucial step in obtaining high-purity C_2H_4 and C_3H_6 is the removal of the main impurity C_2H_6 and recovery of C_3H_6. This is typically achieved through energy-intensive cryogenic cyclic distillation at high pressure, due to their similar physicochemical properties.[3,4] In the industrial field of polymerization, high-purity C_2H_4 and C_3H_6 are desirable, with a purity of over 99.9% and 99.5%, respectively. With the growing demand for C_2H_4 and C_3H_6, exceeding 300 million tons produced in 2023,[5,6] it is vital to replace the energy-intensive distillation methods with more energy-efficient, cost-effective, and environmentally friendly alternatives. Among these methods, adsorption and separation technology utilizing porous materials holds great promise.[4,7–14]

Metal–organic frameworks (MOFs), as a new class of crystalline porous materials, have been developed for adsorptive separation due to their high modularity, exceptional porosity, and diverse functionality.[3,8,15–18] To achieve a simplified C_2H_4 and C_3H_6 purification procedure, the MOF structure must exhibit graded uptake for C_2H_4, C_2H_6 and C_3H_6, with high selectivity and capture capability. Most MOFs have been reported to preferentially adsorb C_2H_4 over C_2H_6 because the incorporation of C_2H_4 binding sites such as unsaturated metal sites into MOF structures is much more easily achieved.[19–21] However, these C_2H_4-selective MOFs are not ideal adsorbents in practical MTO separation as the pure C_2H_4 product must be obtained from the additional desorption process. Thus the development of C_2H_6-selective MOFs to produce the pure C_2H_4 product directly at the outlet is highly desired. For C_3H_6/C_2H_4 separation, previous reports demonstrated that the strategy of utilizing polar functional groups such as open metal sites (OMSs) in MOFs is feasible due to the higher acidity and more –CH groups in C_3H_6 in comparison to C_2H_4.[1,22] However, this strategy is paradoxical to the C_2H_6-selective MOFs because the OMSs in MOFs prefer to interact strongly with C_2H_4 instead of C_2H_6, leading to preferential adsorption of C_2H_4 over C_2H_6, while C_2H_4 purification and C_3H_6 recovery are both important in order to produce high-purity C_2H_4 and C_3H_6 products in the MTO process. Therefore, the

[a]Jiangsu Key Laboratory of Biomedical Materials, School of Chemistry and Materials Science, Nanjing Normal University, Nanjing 210023, China. E-mail: leigan@nnu.edu.cn

[b]School of Chemistry and Chemical Engineering, Liaocheng University, Liaocheng, 252059, China

[c]State Key Laboratory of Separation Membranes and Membrane Processes, School of Chemistry and Chemical Engineering, Tiangong University, Tianjin 300387, China

development of MOF materials for the efficient separation of both C_2H_6/C_2H_4 and C_3H_6/C_2H_4 is a significant challenge.

Recent reports have indicated that enhancing the nonpolarity of the pore surface in MOFs can facilitate the selective adsorption of C_2H_6 over C_2H_4.[23–27] This is because of the higher polarizability of C_2H_6 (44.7×10^{-25} cm^3) compared to that of C_2H_4 (42.52×10^{-25} cm^3).[23] At the same time, nonpolar pores generated by aromatic rings can offer more and stronger C–H$\cdots\pi$ interactions, resulting in enhanced paraffin affinity and selective C_2H_6 adsorption.[28–30] On the other hand, as aromatic moieties such as benzene rings possess delocalized π electrons, the pore surface decorated with benzene rings can provide stronger $\pi\cdots\pi$ interactions between the host and C_3H_6 with a conjugated π system in comparison to C_2H_4 molecules.[31] For example, Chen *et al.* reported that a C_3H_6-selective MOF ZJNU-401 exhibited preferential C_3H_6 adsorption and good C_3H_6/C_2H_4 selectivity, which can be attributed to suitable pore size and benzene ring decorated pore walls.[27] Therefore, we speculate that the MOF structure with a nonpolar pore surface decorated by benzene rings and without OMSs could realize the efficient separation of both C_3H_6/C_2H_4 and C_2H_6/C_2H_4 mixtures.

Additionally, the practical application of high-performance MOFs faces several limitations, primarily high costs, challenges in scalability, and potential performance degradation. Ligand design is crucial for achieving desired structures and properties, but it often leads to significantly increased costs for adsorbents. The raw materials for synthesizing organic ligands can cost tens of dollars per gram, and the production of MOF adsorbents typically requires long reaction times, derailing scalable manufacturing. For example, the C_2H_6-selective benchmark MOF ZNU-10 is synthesized from the reaction of $Cu(NO_3)_2\cdot 3H_2O$ and mixed linkers *p*-$C_2B_{10}H_{10}$–$(COOH)_2$ and DABCO in DMF/MeOH/H_2O solution, with the price not less than $7 per gram.[32] Recently, Hou's group developed a high performance MOF adsorbent, MAC-4, which combines isophthalic acid and 3,5-dimethyl-1,2,4-triazole, and synthesis can be scaled-up with a cost as low as 1.35 $ per gram.[24] The scale-up synthesis of MAC-4 is not an environment-friendly protocol due to the use of DMF solvent, and a sustainable synthesis process can accelerate the commercialization of MOF materials, such as CALF-20,[33,34] MIL-100(Fe),[35,36] *etc.* To advance the industrial application of MOF adsorbents, it is essential to explore options that involve simple, green synthesis processes and very low costs, ensuring high scalability and practicality.

Taking above into consideration, herein we present an efficient C_3H_6- and C_2H_6-selective MOF adsorbent, Zn-hba, enabling the one-step purification of C_2H_4 and efficient recovery of C_3H_6 for the separation of MTO products. Zn-hba is synthesized using the common cheap ligand 4-hydroxybenzoic acid (HBA) and the late transition metal zinc (Zn) through a simple and scaled-up synthesis process, achieving a high yield of 42% (based on Zn) (see the Synthetic section for the detailed procedure). The simple structure avoids the existence of OMSs and features dense, periodic quadrate channels decorated with nonpolar benzene rings, facilitating efficient separation of $C_2H_6/C_2H_4/C_3H_6$ mixtures without performance degradation after cycling measurements. Zn-hba exhibits preferential adsorption of C_2H_6 and C_3H_6 over C_2H_4 with a record-high C_3H_6 packing density (257.54 g L^{-1}) at 1 kPa and extreme high C_2H_6 packing density (186.94 g L^{-1}) at 10 kPa. The Ideal Adsorption Solution Theory (IAST) selectivity for C_2H_6/C_2H_4 and C_3H_6/C_2H_4 is calculated to be 2.41 and 11.73, respectively. Theoretical calculations reveal that the stronger binding affinity for C_3H_6 and C_2H_6 over C_2H_4 between the nonpolar pore surface and guest molecules is responsible for the C_3H_6- and C_2H_6-selective adsorption. Breakthrough experiments confirm the good separation performance of Zn-hba for C_2H_6/C_2H_4 and C_3H_6/C_2H_4 mixtures even under humid conditions. Moreover, Zn-hba could separate the ternary $C_2H_6/C_3H_6/C_2H_4$ mixtures to produce high-purity C_2H_4 (>99.9%) and C_3H_6 (>99.5%) with a productivity of 3.32 and 19.42 L kg^{-1}, respectively. In addition, all reagents used for the synthesis of Zn-hba are commercially available and extremely low cost. Despite the fact that the synthesis is not very sustainable, Zn-hba exhibits a significant cost advantage. The cost per gram of Zn-hba is as low as $0.14, making it comparable to that of commercial zeolites and nearly one-tenth of the price of MAC-4.

Results and discussion

Synthesis and characterization

The evaporation of methanol in the *n*-amyl alcohol/MeOH solution containing $Zn(OAc)_2\cdot 2H_2O$ and 4-hydroxy benzoic acid (hba) yielded colorless needle-like crystals of Zn-hba according to the literature.[37] The scale-up synthesis of Zn-hba also has been investigated *via* using an alternative simple protocol. As shown in Fig. S1, *n*-amyl alcohol was added into the MeOH solution containing $Zn(OAc)_2\cdot 2H_2O$ and 4-hydroxy benzoic acid under heating conditions at 100 °C in a round flask to obtain the final microcrystalline Zn-hba sample, and the solvent methanol was recovered during the reaction. These mild synthetic conditions and simple synthetic procedures can produce around 5 g of Zn-hba with a high yield of 42% in 12 hours through one single reaction. Moreover, compared to most porous MOFs applied to gas adsorptive separation, the raw materials for synthesis of Zn-hba are commercially available and the price is very low. The cost of the Zn-hba material is calculated to be $0.14 per kg (Table S1), which makes it comparable to that of commercial zeolites and nearly one-tenth of the price of MAC-4. It is noted that Zn-hba made with this scalable synthesis method exhibited good crystallinity and high phase purity, which was confirmed by powder X-ray diffraction (PXRD) measurements (Fig. S2).

The network of Zn-hba is constructed with 1D tetrahedral zinc(II)-based helical chains as the second building unit (SBU) connected to μ_2-phenolate and carboxylate groups. The hba linkers extend from the metal chains in four directions and perpendicular to the 1D helical chains. Furthermore, each hba linker is linked to two adjacent helical chains, resulting in a 3D structure of 9.1 Å × 9.1 Å square channels with a formula of $Zn(hba)\cdot xH_2O$ (Fig. 1). Based on the Platon calculation, the framework of Zn-hba exhibits a porosity of 37.9%. Additionally, the 1D square channels in the 001 direction are decorated with

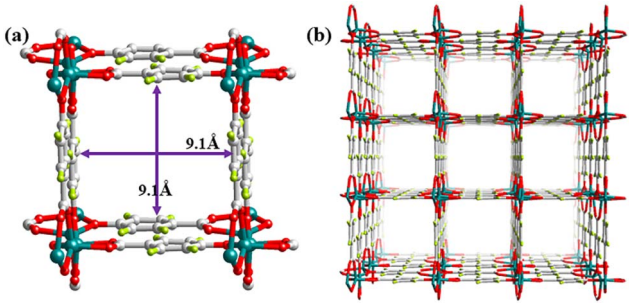

Fig. 1 (a) Schematic illustration of a 1 D channel decorated with benzene rings and (b) the 3D network of Zn-hba.

aromatic moieties and the open metal sites are completely avoided in the structure, providing a nonpolar pore surface that facilitates selective C_3H_6 and C_2H_6 adsorption over C_2H_4 for Zn-hba. The PXRD pattern of as-synthesized samples is consistent with the corresponding simulated one from single crystal data, indicating that its bulk product was pure phase (Fig. S2). The thermogravimetric analysis (TGA) indicated that Zn-hba can be completely desolvated (Fig. S3), facilitating the examination of their permanent porosities. Nitrogen (N_2) adsorption isotherms at 77 K showed type-I curves of Zn-hba (Fig. S4), with a saturated loading of 177 $cm^3\ g^{-1}$, indicating a close Brunauer–Emmett–Teller (BET) surface area of 672 $m^2\ g^{-1}$, and corresponding experimental pore volume of 0.259 $cm^3\ g^{-1}$. The pore size distribution of 8 Å agrees with the calculated results from the crystal structure. Moreover, the chemical stability of Zn-hba has been examined. The variable temperature VT-PXRD measurements show that Zn-hba can retain its structural rigidity up to 500 °C (Fig. S5). This ultrahigh thermal stability is rare among MOFs and surpasses that of all Zn–MOFs[23,24,38–42] to the best of our knowledge. Besides, Zn-hba also exhibits high stability in humid air for one week (Fig. S6). Overall, these data demonstrate that Zn-hba is a robust porous MOF for gas adsorption.

Gas adsorption properties

The well-developed channels combined with the nonpolar pore surface and high stability encouraged us to investigate the gas adsorption performance of Zn-hba for light hydrocarbons. Single-component gas adsorption isotherms for C_2H_6, C_2H_4 and C_3H_6 were collected on Zn-hba small-scale samples at 273/298 K under 100 kPa. As illustrated in Fig. 2a and b, the maximum uptake of 75.9/67.3 $cm^3\ g^{-1}$ for C_2H_6 and 77.2/71.2 $cm^3\ g^{-1}$ for C_3H_6 at 273/298 K, were both much higher than that of 73.4/61.7 $cm^3\ g^{-1}$ for C_2H_4. Thus the adsorption capacity is in the order of $C_3H_6 > C_2H_6 > C_2H_4$, indicating a reversed adsorption behaviour in Zn-hba, which is quite rare among reported MOFs.[23–25,27,43] Remarkably, Zn-hba exhibits abundant C_3H_6 and C_2H_6 adsorption at extremely low pressure at 273 or 298 K (Fig. 2c and d). The adsorption of C_3H_6 is record-high with an uptake of 38.91 $cm^3\ g^{-1}$ at 1 kPa and 298 K, being the highest among all MOFs for C_3H_6-selective adsorption (Table S2). The adsorption capacity of C_2H_6, with a value of 39.54 $cm^3\ g^{-1}$ at 10 kPa and 298 K, is also the highest among most MOFs for C_2H_6-selective

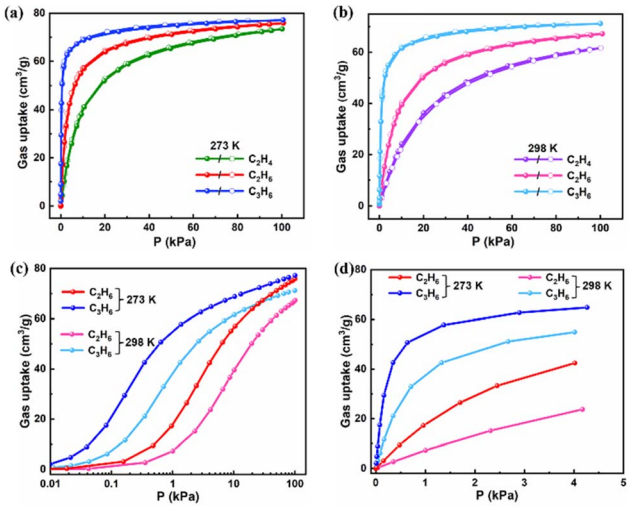

Fig. 2 Gas adsorption isotherms of C_2H_4, C_2H_6, and C_3H_6 on small-scale Zn-hba at (a) 273 K and (b) 298 K; logarithmic-scale plots within the range of (c) 0–100 kPa and (d) 0–5 kPa at 273/298 K.

adsorption, except slightly lower than that of NTU-70P (40.3 $cm^3\ g^{-1}$)[40] (Table S3). Afterwards, the packing density of C_3H_6 was calculated to be 258 g L^{-1}, which is the highest one at 1 kPa when compared with that of reported MOFs (Table S2). The C_2H_6 packing density was estimated to be 187 g L^{-1}, being the second highest value at 10 kPa in comparison to other MOFs (Table S3). It is worth noting that the C_2H_6 and C_3H_6 packing density outperforms that of some of the best-performing MOF materials such as Zn-BPZ-TATB,[23] MAC-4 (ref. 24) and ZJUN-401.[27] Meanwhile, the adsorption of C_2H_4, especially in the low-pressure regions, is quite low. Moreover, it is also clear that the slopes of C_2H_6 and C_3H_6 adsorption isotherms are much steeper than that of C_2H_4, indicating that the adsorption affinity in Zn-hba follows the order of $C_3H_6 > C_2H_6 > C_2H_4$, which suggests that Zn-hba has great potential for $C_3H_6/C_2H_6/C_2H_4$ gas mixture separation in the MTO process. Importantly, the scale-up synthesized Zn-hba exhibits similar adsorption isotherms to C_2H_4, C_2H_6 and C_3H_6 in comparison with the small-scale synthesized single crystal samples (Fig. S7). To further assess the durability of Zn-hba for gas adsorption performance, we conducted cyclic adsorption experiments. The continuous C_2H_6, C_2H_4 and C_3H_6 adsorption measurements without reactivation at 298 K showed the uptake of C_2H_6, C_2H_4 and C_3H_6 and no obvious decrease for atleast five adsorption cycles (Fig. S8), demonstrating excellent recyclability and regeneration capability of the material. The high crystallinity of Zn-hba post-experimentation was confirmed by PXRD analysis and N_2 adsorption results (Fig. S9). No obvious change in PXRD peaks and N_2 adsorption curves at 77 K (Fig. S9) was observed, indicating that Zn-hba possesses excellent durability and recyclability for this gas adsorption.

The adsorption enthalpies (Q_{st}) were determined from sorption isotherms *via* the Clausius–Clapeyron equation at 298 K and 273 K to appraise the interaction strengths of the framework for C_2H_4, C_2H_6 and C_3H_6. The Q_{st} values at zero-coverage of C_3H_6, C_2H_6 and C_2H_4 were computed to be 31.0,

26.9 and 26.1 kJ mol^{-1} (Fig. S10), respectively, corroborating that C_3H_6 and C_2H_6 have stronger affinity with the framework than C_2H_4. It is noteworthy that the Q_{st} values of all three gases are relatively low due to the nonpolar pore surface of Zn-hba, indicating that the regeneration treatment is simple and consumes a low amount of energy. In fact, a simple activation treatment at 373 K for 30 minutes prior to each cycle was sufficient to regenerate fully reproducible adsorption profiles for C_3H_6, C_2H_6 and C_2H_4.

As discussed above, Zn-hba exhibits a higher adsorption capacity of C_3H_6 and C_2H_6 than that of C_2H_4, making it a potential material for C_2H_4 purification in MTO application. Thus we have examined the separation of binary gas mixtures in the range of 0–100 kPa using ideal adsorption solution theory (IAST). As shown in Fig. 3a and S11, Zn-hba exhibits high selectivity values of 2.41/2.49/2.50, and 2.61/2.70/2.7 for 1/1, 1/9, and 1/15 C_2H_6/C_2H_4 mixtures at 298/273 K and 100 kPa, respectively.

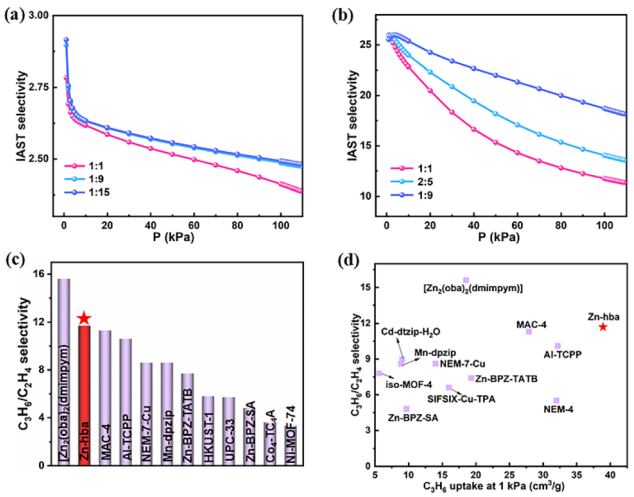

Fig. 3 IAST selectivity curves of Zn-hba for (a) C_2H_6/C_2H_4 and (b) C_3H_6/C_2H_4 mixtures at 298 K; (c) comparisons of the selectivity in Zn-hba and some benchmark materials for C_3H_6/C_2H_4 (1/1); (d) comparison of C_3H_6 uptake at 1 kPa and C_3H_6/C_2H_4 IAST selectivity for Zn-hba and other benchmark materials.

The selectivity for the equimolar C_2H_6/C_2H_4 mixture at 298 K and 100 kPa is comparable to that of many top-performing C_2H_6-selective MOFs such as ZIF-8,[44] PCN-250,[45] and MAC-4 (ref. 24) (Fig. S12). For C_3H_6/C_2H_4 mixtures, the selectivity values were estimated to be 11.73/14.05/18.70, and 16.33/18.80/22.93 for 1/1, 2/5, and 1/9 C_3H_6/C_2H_4 mixtures at 298/273 K and 100 kPa, respectively (Fig. 3b and S13). Notably, this selectivity for the equimolar C_3H_6/C_2H_4 mixture at 298 K and 100 kPa is the highest among reported C_3H_6-selective MOFs,[22,23,25,46] but only lower than that of $Zn_2(oba)_2(dmipym)$ (15.6)[26] (Fig. 3c and d).

To in-depth understand the adsorption mechanism of C_3H_6, C_2H_6 and C_2H_4 in Zn-hba, theoretical calculations based on first-principles dispersion-corrected density functional theory (DFT-D) were performed to reveal the host–guest interactions between the framework and adsorbates. As illustrated in Fig. 4 and S14, the preferential adsorption sites of C_3H_6, C_2H_6 and C_2H_4 are similar and located within the square channels. In Zn-hba, one C_2H_4 molecule interacts with two carboxylate groups in hba linkers *via* four C–H···O interactions (2.84, 3.13, 3.64 and 3.65 Å) and two aromatic moieties *via* three C–H···π interactions (3.41, 3.61 and 3.74 Å), providing a static binding energy of −38.73 kJ mol^{-1} (Fig. 4a). For C_2H_6, there are five C–H···O interactions (2.84, 2.90, 3.27, 3.29 and 3.81 Å) between the gas molecule and carboxylates, and four C–H···π interactions (2.98, 3.41, 3.59 and 3.88 Å). The average binding energy for these C_2H_6 adsorption sites is calculated to be −44.94 kJ mol^{-1}, indicating a stronger binding affinity between the alkane adsorbate and nonpolar pore surface with aromatic rings (Fig. 4b). Due to more hydrogen atoms and the larger size of the C_3H_6 molecule, there are more contacts involving C–H···O interactions (2.78, 2.82, 2.83, 3.26, 3.65 and 3.79 Å) between C_3H_6 and carboxylate/hydroxyl groups in hba and C–H···π interactions (3.03, 3.57, 3.62, 3.67 and 3.95 Å) between C_3H_6 and benzene rings, with a much stronger binding energy of −50.87 kJ mol^{-1}, resulting in an enhanced host–guest interaction to facilitate the capture of propylene in the Zn-hba framework (Fig. 4c). These DFT calculation results provide a rational explanation for the experimental observations of preferential adsorption of C_2H_6 and C_3H_6 over C_2H_4. Apart from the

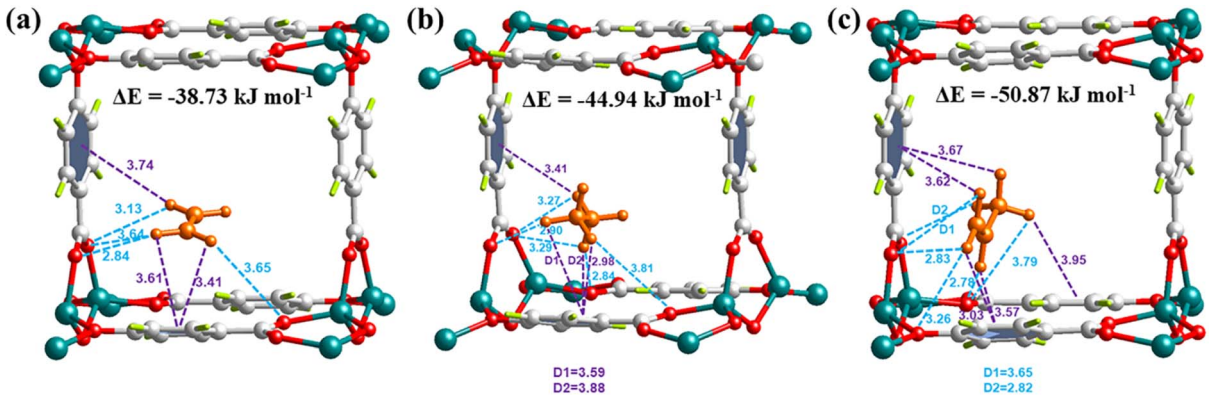

Fig. 4 The DFT-calculated configurations of (a) C_2H_4, (b) C_2H_6, and (c) C_3H_6 in Zn-hba. Green, Zn; red, O; gray, C; light green, H; orange, adsorbed gas molecules.

thermodynamics of host–guest interactions, the kinetic adsorption effect is also very important for assessing porous materials' performance. Therefore, the adsorption kinetics were also studied using molecular dynamics (MD) simulations.

As shown in Fig. S15, the diffusion coefficients (D_s) of the three gas molecules were estimated to be 1.73×10^{-8} m^2 s^{-1} for C_2H_4, 1.27×10^{-8} m^2 s^{-1} for C_2H_6 and 1.05×10^{-8} m^2 s^{-1} for C_3H_6, respectively, demonstrating faster diffusion behavior of C_2H_4 and C_2H_6 over C_3H_6. Additionally, kinetic mechanisms were investigated *via* adsorption experiments (Fig. S16). The adsorption rates were collected from the adsorption analyzer and the experimental kinetic diffusion coefficients (K_s) were determined to be 4.3×10^{-2}, 2.5×10^{-2} and 1.1×10^{-2} for C_2H_4, C_2H_6 and C_3H_6, respectively. The larger K_s of C_2H_6 and C_3H_6 than C_2H_4 indicates the faster adsorption kinetics of C_2H_6 and C_3H_6 compared to that of C_2H_4 in Zn-hba. The experimental data are consistent with the MD simulation results, demonstrating that smaller adsorbate molecular size causes faster guest diffusion. In brief, we thus reason that the preferential adsorption of C_2H_6 and C_3H_6 over C_2H_4 is determined by thermodynamic mechanisms instead of kinetic mechanisms.

Breakthrough experiments

To evaluate the practical C_2H_6/C_2H_4 separation performance of Zn-hba, dynamic breakthrough experiments were performed on Zn-hba large-scale samples for C_2H_6/C_2H_4 (v/v, 5/5, 1/9, and 1/15) mixtures using Ar as the carrier gas with a total flow rate of 10 mL min^{-1} at 298 K. C_2H_4 eluted first from the column to produce the high-purity C_2H_4 (>99.9%) product (Fig. 5a and S17). The separation factor was estimated to be 2.36, 2.75 and 2.98 for 5/5, 1/9, and 1/15 C_2H_6/C_2H_4 mixtures, respectively, which are similar to the IAST selectivities. The separation performance of the Zn-hba material for C_3H_6/C_2H_4 (v/v: 5/5, 2/5, and 1/9) mixtures was also verified under similar conditions. As shown in Fig. 5b and S18, C_2H_4 passed through the column rapidly while C_3H_6 flowed out slowly at 92/163/172 min g^{-1}, respectively. Notably, these breakthrough time intervals for C_3H_6 in Zn-hba are the longest among most MOFs for C_3H_6/C_2H_4 separation, such as Zn-BPZ-TATB,[23] MAC-4 (ref. 24) and ZJNU-401,[27] suggesting the excellent separation ability of Zn-hba for C_3H_6/C_2H_4. Subsequently, the polymer-grade C_2H_4 (>99.95%) was estimated to be 56.49/85.17/120.00 L kg^{-1}, superior to those of $[Zn_2(oba)_2(dmimpym)]$,[26] Zn-BPZ-SA[47] under similar conditions. As pure C_3H_6 is another very important product in the MTO process, high-purity C_3H_6 (>99.94%) can be obtained by the desorption experiments *via* Ar purging. As a result, the productivity of C_3H_6 for the C_3H_6/C_2H_4 mixture (v/v, 5/5) was calculated to be 25.81 L kg^{-1}, which is comparable to that of Cd-dtzip-H_2O (Fig. S19).[48] Furthermore, Zn-hba also exhibited good C_3H_6/C_2H_4 separation performance under humid conditions. The breakthrough time was almost the same for 3 cycles of breakthrough experiments under 50% and 100% humid conditions (Fig. S20 and S21), indicating the excellent moisture resistance of Zn-hba for C_3H_6/C_2H_4 separation. The structural stability of Zn-hba was confirmed by PXRD and N_2 adsorption results (Fig. S22 and S23), proving its excellent humidity-resistant recyclability and durability. Additionally, as illustrated in Fig. S24 and S25, Zn-hba shows good recycling performance for the separation of equimolar C_2H_6/C_2H_4 and C_3H_6/C_2H_4 mixtures at 298 K, making it a potential material for industrial C_2H_4 purification.

During the real industrial process, there are some light hydrocarbons in the MTO products, which is a significant challenge for high-purity C_3H_6 recovery and C_2H_4 purification. Therefore, the dynamic breakthrough measurements for ternary $C_2H_6/C_3H_6/C_2H_4$ mixtures with various ratios were performed at 298 K to evaluate the separation performance of Zn-hba. As shown in Fig. 5c, for the 33.3/33.3/33.3 ternary mixtures, C_2H_4 passed through the column rapidly to produce high-purity C_2H_4 (>99.9%) with a productivity of 3.32 L kg^{-1}, following by C_2H_6 detected from the outlet, while C_3H_6 occurred until around 46 min. Then the desorption experiments were performed by purging with He gas with a flow rate of 5 mL min^{-1} at 373 K. As a result, 19.42 L kg^{-1} C_3H_6 (>99.5%) were recovered from the ternary mixtures in one single adsorption/desorption process. Moreover, when the ratios of ternary mixtures were set up to be 1/9/90 and 2/10/25, Zn-hba still exhibited efficient separation performance (Fig. S26 and S27), making it an excellent adsorbent for C_2H_4 purification and C_3H_6 recovery in MTO product separation. Overall, Zn-hba obtains good scores in uptake at low pressure, IAST selectivity, scalability, price and separation under humidity, which highlights its high promise for real industrial separation (Fig. 5d).

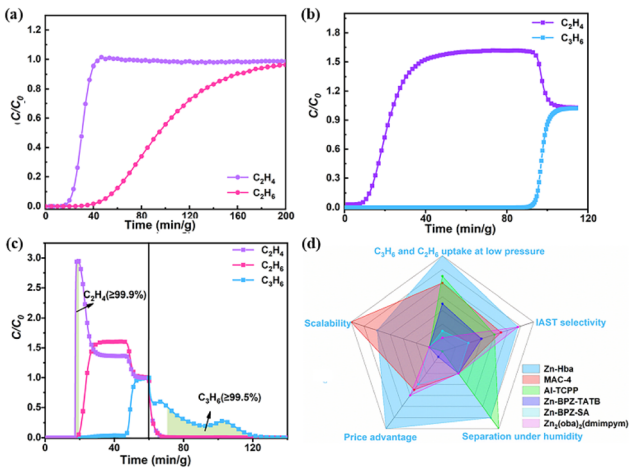

Fig. 5 (a) Breakthrough curves for C_2H_6/C_2H_4 (v/v, 1/15) mixtures at 298 K; (b) breakthrough curves for C_3H_6/C_2H_4 (v/v, 5/5) mixtures at 298 K; (c) breakthrough curves for the $C_2H_6/C_3H_6/C_2H_4$ mixture (v/v/v, 33.3/33.3/33.3) at 298 K; (d) comprehensive comparisons for Zn-hba and other porous materials.

Conclusions

In summary, we developed a scalable and simple synthetic method to produce a low-cost and robust MOF, Zn-hba. Its production cost is only \$0.14 per kg, significantly lower than that of most reported MOF materials. Moreover, the low polarity pore surface promotes that Zn-hba prefers adsorbing C_3H_6 and C_2H_6 over C_2H_4 and yields a record-high propylene packing

density and exceptionally high ethane packing density at low pressure, which leads to significant C_3H_6/C_2H_4 and C_2H_6/C_2H_4 selectivities, exceeding that of most C_3H_6 and C_2H_6-selective MOFs. DFT calculations reveal that there are more multiple supramolecular interactions and a stronger binding affinity between the nonpolar pore surface of Zn-hba and C_3H_6 and C_2H_6 in comparison to C_2H_4. Breakthrough experiments confirm the good separation performance of Zn-hba for C_2H_6/C_2H_4 and C_3H_6/C_2H_4 mixtures with the longest breakthrough time intervals. More importantly, Zn-hba maintains its C_3H_6/C_2H_4 separation ability after multiple cycles of breakthrough experiments at high humidity. In addition, Zn-hba can produce polymer-grade C_2H_4 (>99.9%) and high-purity C_3H_6 (>99.5%) from ternary $C_3H_6/C_2H_6/C_2H_4$ mixtures *via* one adsorption–desorption process. In general, the synthetic feasibility, low-cost, and easy scalability in combination with good separation performance make Zn-hba the most promising material for industrial gas separation. This work highlights the significance of a nonpolar pore environment in MOF materials to facilitate the challenging separation and practical industrial application.

Author contributions

L. G. and H.-J. Y. conceived the idea. Y.-Y. Z. carried out the experiments and analyzed the data. L. G. and C.-Z. X. wrote the manuscript. All authors contributed to the preparation of the manuscript.

Conflicts of interest

There are no conflicts to declare.

Data availability

The data supporting this article have been included as part of the SI. Supplementary information is available: Synthetic procedure, experimental details, all characterisation data, additional adsorption and separation data. See DOI: **https://doi.org/10.1039/d5sc03946k**.

Acknowledgements

We acknowledge the financial support from the National Natural Science Foundation of China (Grant No. 22301138) and Jiangsu Specially Appointed Professorship, and the startup funding from Nanjing Normal University.

Notes and references

1 W. Fan, X. Wang, X. Zhang, X. Liu, Y. Wang, Z. Kang, F. Dai, B. Xu, R. Wang and D. Sun, Fine-Tuning the Pore Environment of the Microporous Cu-MOF for High Propylene Storage and Efficient Separation of Light Hydrocarbons, *ACS Cent. Sci.*, 2019, **5**, 1261–1268.

2 J. Liu, J. Miao, S. Ullah, K. Zhou, L. Yu, H. Wang, Y. Wang, T. Thonhauser and J. Li, A Water-Resistant Hydrogen-Bonded Organic Framework for Ethane/Ethylene Separation in Humid Environments, *ACS Mater. Lett.*, 2022, **4**, 1227–1232.

3 K. Adil, Y. Belmabkhout, R. S. Pillai, A. Cadiau, P. M. Bhatt, A. H. Assen, G. Maurin and M. Eddaoudi, Gas/vapour separation using ultra-microporous metal–organic frameworks: insights into the structure/separation relationship, *Chem. Soc. Rev.*, 2017, **46**, 3402–3430.

4 D. S. Sholl and R. P. Lively, Seven chemical separations to change the world, *Nature*, 2016, **532**, 435–437.

5 Z. Di, C. Liu, J. Pang, S. Zou, Z. Ji, F. Hu, C. Chen, D. Yuan, M. Hong and M. Wu, A Metal-Organic Framework with Nonpolar Pore Surfaces for the One-Step Acquisition of C_2H_4 from a C_2H_4 and C_2H_6 Mixture, *Angew. Chem., Int. Ed.*, 2022, **61**, e202210343.

6 P. Hu, J. Hu, H. Liu, H. Wang, J. Zhou, R. Krishna and H. Ji, Quasi-Orthogonal Configuration of Propylene within a Scalable Metal–Organic Framework Enables Its Purification from Quinary Propane Dehydrogenation Byproducts, *ACS Cent. Sci.*, 2022, **8**, 1159–1168.

7 Y.-J. Tian, C. Deng, Y.-L. Peng, X. Zhang, Z. Zhang and M. J. Zaworotko, State of the art, challenges and prospects in metal–organic frameworks for the separation of binary propylene/propane mixtures, *Coord. Chem. Rev.*, 2024, **506**, 215697.

8 L. Yang, S. Qian, X. Wang, X. Cui, B. Chen and H. Xing, Energy-efficient separation alternatives: metal–organic frameworks and membranes for hydrocarbon separation, *Chem. Soc. Rev.*, 2020, **49**, 5359–5406.

9 X.-W. Zhang, C. Wang, Z.-W. Mo, X.-X. Chen, W.-X. Zhang and J.-P. Zhang, Quasi-open Cu(I) sites for efficient CO separation with high O_2/H_2O tolerance, *Nat. Mater.*, 2024, **23**, 116–123.

10 K.-J. Chen, D. G. Madden, S. Mukherjee, T. Pham, K. A. Forrest, A. Kumar, B. Space, J. Kong, Q.-Y. Zhang and M. J. Zaworotko, Synergistic sorbent separation for one-step ethylene purification from a four-component mixture, *Science*, 2019, **366**, 241–246.

11 J. Cui, Z. Zhang, L. Yang, J. Hu, A. Jin, Z. Yang, Y. Zhao, B. Meng, Y. Zhou, J. Wang, Y. Su, J. Wang, X. Cui and H. Xing, A molecular sieve with ultrafast adsorption kinetics for propylene separation, *Science*, 2024, **383**, 179–183.

12 B. Sun, C. Zeng, S. Deng, Y. Gu, L. Gan and H. Yang, Adsorption Kinetics-Driven Humidity-Resistant C_2H_2/CO_2 Separation by a Hydrophilic Metal–Organic Framework, *Chem. Mater.*, 2025, **37**, 1154–1159.

13 Y. Qi, C. Xue, Y. Zhang, Y. Huang, H. Huang, L. Gan and H. Yang, Nonpolar Pore Confinement within Metal–Organic Frameworks for Xe/Kr Separation, *ACS Mater. Lett.*, 2025, **7**, 1488–1495.

14 C. Xue, H. Peng, J. Hou and K. Qu, Pore space partition on a sulfonate-rich metal–organic framework for purification of methane from natural gas, *Chem. Commun.*, 2025, **61**, 8244–8247.

15 X.-R. Tian, Z.-Y. Jiang, S.-L. Hou, H.-S. Hu, J. Li and B. Zhao, A Strong-Acid-Resistant $[Th_6]$ Cluster-Based Framework for Effectively and Size-Selectively Catalyzing Reductive

Amination of Aldehydes with N,N-Dimethylformamide, *Angew. Chem., Int. Ed.*, 2023, **62**, e202301764.

16 G. Hu, Q. Liu, Y. Zhou, W. Yan, Y. Sun, S. Peng, C. Zhao, X. Zhou and H. Deng, Extremely Large 3D Cages in Metal–Organic Frameworks for Nucleic Acid Extraction, *J. Am. Chem. Soc.*, 2023, **145**, 13181–13194.

17 Q. Yin, Z. Song, S. Yang, G.-D. Wang, Y. Sui, J. Qi, D. Zhao, L. Hou and Y.-Z. Li, A nickel-based metal–organic framework as a new cathode for chloride ion batteries with superior cycling stability, *Chem. Sci.*, 2023, **14**, 5643–5649.

18 M. Ding, R. W. Flaig, H.-L. Jiang and O. M. Yaghi, Carbon capture and conversion using metal–organic frameworks and MOF-based materials, *Chem. Soc. Rev.*, 2019, **48**, 2783–2828.

19 L. Yang, Y. Wang, Y. Chen, J. Yang, X. Wang, L. Li and J. Li, Microporous metal-organic framework with specific functional sites for efficient removal of ethane from ethane/ethylene mixtures, *Chem. Eng. J.*, 2020, **387**, 124137.

20 D. Lv, R. Shi, Y. Chen, Y. Wu, H. Wu, H. Xi, Q. Xia and Z. Li, Selective Adsorption of Ethane over Ethylene in PCN-245: Impacts of Interpenetrated Adsorbent, *ACS Appl. Mater. Interfaces*, 2018, **10**, 8366–8373.

21 T.-L. Hu, H. Wang, B. Li, R. Krishna, H. Wu, W. Zhou, Y. Zhao, Y. Han, X. Wang, W. Zhu, Z. Yao, S. Xiang and B. Chen, Microporous metal–organic framework with dual functionalities for highly efficient removal of acetylene from ethylene/acetylene mixtures, *Nat. Commun.*, 2015, **6**, 7328.

22 L. Zhang, L.-N. Ma, G.-D. Wang, L. Hou, Z. Zhu and Y.-Y. Wang, A new honeycomb MOF for C_2H_4 purification and C_3H_6 enrichment by separating methanol to olefin products, *J. Mater. Chem. A*, 2023, **11**, 2343–2348.

23 G.-D. Wang, Y.-Z. Li, W.-J. Shi, L. Hou, Y.-Y. Wang and Z. Zhu, Active Sites Decorated Nonpolar Pore-Based MOF for One-step Acquisition of C_2H_4 and Recovery of C_3H_6, *Angew. Chem., Int. Ed.*, 2023, **62**, e202311654.

24 G.-D. Wang, Y.-Z. Li, R. Krishna, W.-Y. Zhang, L. Hou, Y.-Y. Wang and Z. Zhu, Scalable Synthesis of Robust MOF for Challenging Ethylene Purification and Propylene Recovery with Record Productivity, *Angew. Chem., Int. Ed.*, 2024, **63**, e202319978.

25 J. Xiao, Z. Zhu, M. Zhang, Y. Huang, T. C. Zhang and S. Yuan, Efficient One-Step Purification of Methanol-to-Olefin Products Using a Porphyrinyl MOF to Achieve Record C_2H_4 and C_3H_6 Productivity, *ACS Appl. Mater. Interfaces*, 2025, **17**, 21630–21642.

26 Y.-Z. Li, G.-D. Wang, R. Krishna, Q. Yin, D. Zhao, J. Qi, Y. Sui and L. Hou, A separation MOF with O/N active sites in nonpolar pore for one-step C_2H_4 purification from C_2H_6 or C_3H_6 mixtures, *Chem. Eng. J.*, 2023, **466**, 143056.

27 J. Li, Z. Song, X. Zhou, X. Wang, M. Feng, D. Wang and B. Chen, Reticular chemistry guided function customization: a case study of constructing low-polarity channels for efficient C_3H_6/C_2H_4 separation, *Chem. Sci.*, 2025, **16**, 7411–7417.

28 R.-B. Lin, H. Wu, L. Li, X.-L. Tang, Z. Li, J. Gao, H. Cui, W. Zhou and B. Chen, Boosting Ethane/Ethylene Separation within Isoreticular Ultramicroporous Metal–Organic Frameworks, *J. Am. Chem. Soc.*, 2018, **140**, 12940–12946.

29 C. He, Y. Wang, Y. Chen, X. Wang, J. Yang, L. Li and J. Li, Modification of the pore environment in UiO-type metal-organic framework toward boosting the separation of propane/propylene, *Chem. Eng. J.*, 2021, **403**, 126428.

30 X. Zhang, L. Li, J.-X. Wang, H.-M. Wen, R. Krishna, H. Wu, W. Zhou, Z.-N. Chen, B. Li, G. Qian and B. Chen, Selective Ethane/Ethylene Separation in a Robust Microporous Hydrogen-Bonded Organic Framework, *J. Am. Chem. Soc.*, 2020, **142**, 633–640.

31 X. Wang, Y. Wu, J. Peng, Y. Wu, J. Xiao, Q. Xia and Z. Li, Novel glucosamine-based carbon adsorbents with high capacity and its enhanced mechanism of preferential adsorption of C_2H_6 over C_2H_4, *Chem. Eng. J.*, 2019, **358**, 1114–1125.

32 L. Wang, S. Wu, J. Hu, Y. Jiang, J. Li, Y. Hu, Y. Han, T. Ben, B. Chen and Y. Zhang, A novel hydrophobic carborane-hybrid microporous material for reversed C_2H_6 adsorption and efficient C_2H_4/C_2H_6 separation under humid conditions, *Chem. Sci.*, 2024, **15**, 5653–5659.

33 D. Chakraborty, A. Yurdusen, G. Mouchaham, F. Nouar and C. Serre, Large-Scale Production of Metal–Organic Frameworks, *Adv. Funct. Mater.*, 2024, **34**, 2309089.

34 J.-B. Lin, T. T. T. Nguyen, R. Vaidhyanathan, J. Burner, J. M. Taylor, H. Durekova, F. Akhtar, R. K. Mah, O. Ghaffari-Nik, S. Marx, N. Fylstra, S. S. Iremonger, K. W. Dawson, P. Sarkar, P. Hovington, A. Rajendran, T. K. Woo and G. K. H. Shimizu, A scalable metal-organic framework as a durable physisorbent for carbon dioxide capture, *Science*, 2021, **374**, 1464–1469.

35 P. Horcajada, S. Surblé, C. Serre, D.-Y. Hong, Y.-K. Seo, J.-S. Chang, J.-M. Grenèche, I. Margiolaki and G. Férey, Synthesis and catalytic properties of MIL-100(Fe), an iron(III) carboxylate with large pores, *Chem. Commun.*, 2007, **27**, 2820–2822.

36 G. Férey, C. Serre, C. Mellot-Draznieks, F. Millange, S. Surblé, J. Dutour and I. Margiolaki, A Hybrid Solid with Giant Pores Prepared by a Combination of Targeted Chemistry, Simulation, and Powder Diffraction, *Angew. Chem., Int. Ed.*, 2004, **43**, 6296–6301.

37 K. F. White, B. F. Abrahams, R. Babarao, A. D. Dharma, T. A. Hudson, H. E. Maynard-Casely and R. Robson, A New Structural Family of Gas-Sorbing Coordination Polymers Derived from Phenolic Carboxylic Acids, *Chem.–Eur. J.*, 2015, **21**, 18057–18061.

38 Y. Gao, M. Zhang, C. Chen, Y. Zhang, Y. Gu, Q. Wang, W. Zhang, Y. Pan, J. Ma and J. Bai, A low symmetry cluster meets a low symmetry ligand to sharply boost MOF thermal stability, *Chem. Commun.*, 2020, **56**, 11985–11988.

39 S. Kusaka, Y. Itoh, A. Hori, J. Usuba, J. Pirillo, Y. Hijikata, Y. Ma and R. Matsuda, Adsorptive-dissolution of O_2 into the potential nanospace of a densely fluorinated metal-organic framework, *Nat. Commun.*, 2024, **15**, 10117.

40 P. Nugent, Y. Belmabkhout, S. D. Burd, A. J. Cairns, R. Luebke, K. Forrest, T. Pham, S. Ma, B. Space, L. Wojtas,

M. Eddaoudi and M. J. Zaworotko, Porous materials with optimal adsorption thermodynamics and kinetics for CO_2 separation, *Nature*, 2013, **495**, 80–84.

41 H. Furukawa, N. Ko, Y. B. Go, N. Aratani, S. B. Choi, E. Choi, A. Ö. Yazaydin, R. Q. Snurr, M. O'Keeffe, J. Kim and O. M. Yaghi, Ultrahigh Porosity in Metal-Organic Frameworks, *Science*, 2010, **329**, 424–428.

42 H. Li, M. Eddaoudi, M. O'Keeffe and O. M. Yaghi, Design and synthesis of an exceptionally stable and highly porous metal-organic framework, *Nature*, 1999, **402**, 276–279.

43 W. Liu, E. Wu, B. Yu, Z. Liu, K. Wang, D. Qi, B. Li and J. Jiang, Reticular Synthesis of Metal-Organic Frameworks by 8-Connected Quadrangular Prism Ligands for Water Harvesting, *Angew. Chem., Int. Ed.*, 2023, **62**, e202305144.

44 Y. Wu, H. Chen, D. Liu, Y. Qian and H. Xi, Adsorption and separation of ethane/ethylene on ZIFs with various topologies: combining GCMC simulation with the ideal adsorbed solution theory (IAST), *Chem. Eng. Sci.*, 2015, **124**, 144–153.

45 Y. Chen, Z. Qiao, H. Wu, D. Lv, R. Shi, Q. Xia, J. Zhou and Z. Li, An ethane-trapping MOF PCN-250 for highly selective adsorption of ethane over ethylene, *Chem. Eng. Sci.*, 2018, **175**, 110–117.

46 D. Geng, M. Zhang, X. Hang, W. Xie, Y. Qin, Q. Li, Y. Bi and Z. Zheng, A 2D metal–thiacalix[4]arene porous coordination polymer with 1D channels: gas absorption/separation and frequency response, *Dalton Trans.*, 2018, **47**, 9008–9013.

47 G.-D. Wang, R. Krishna, Y.-Z. Li, Y.-Y. Ma, L. Hou, Y.-Y. Wang and Z. Zhu, Rational Construction of Ultrahigh Thermal Stable MOF for Efficient Separation of MTO Products and Natural Gas, *ACS Mater. Lett.*, 2023, **5**, 1091–1099.

48 L. Zhang, R.-C. Gao, X. Liu, B. Zhang, L. Hou and Y.-Y. Wang, Unique H_2O Vortex in One New MOF Material Strengthening C_3H_6 Adsorption and Unprecedented Purification from $C_2H_4/C_3H_8/C_3H_6$ Mixtures, *Adv. Funct. Mater.*, 2025, **35**, 2420927.